Biomaterials Science

ROYAL SOCIETY OF CHEMISTRY

PAPER

View Article Online
View Journal | View Issue

Cite this: *Biomater. Sci.*, 2023, **11**, 2566

Supercritical carbon dioxide-decellularized arteries exhibit physiologic-like vessel regeneration following xenotransplantation in rats

Shih-Ying Sung,[a,b] Yi-Wen Lin,[c] Chin-Chen Wu,[d] Chih-Yuan Lin,[b] Po-Shun Hsu,[a,b] Srinivasan Periasamy,[e] Balaji Nagarajan,[f] Dar-Jen Hsieh,[e] Yi-Ting Tsai,*[a,b,g] Chien-Sung Tsai*[a,b,d,g] and Feng-Yen Lin *[g,h,i]

Currently, many techniques are used for decellularization of grafts, including physical, enzymatic, and chemical treatments. Indeed, decellularized xenogenic grafts provide superior outcomes than alternative synthetic conduits. However, vascular grafts produced by these methods are not perfect; their defects include defective vessel wall structures, detergent residues, and the development of aneurysms after grafting. Therefore, it is essential to develop a more appropriate process to produce decellularized vascular grafts. Supercritical carbon dioxide ($ScCO_2$) has been used in decellularization technologies in recent years. It is beneficial for the long-term preservation of tissues and regeneration of new vessels. We have previously reported that $ScCO_2$-produced acellular porcine corneas show excellent biocompatibility following lamellar corneal transplantation in rabbits. In this study, we wanted to use this method to fabricate vascular grafts ($ScCO_2$-decellularized rabbit femoral artery (DFA)) and analyze their efficacy, parameters regarding rejection by the recipient's (ACI/NKyo rats) immune system and biocompatibility, structural regeneration, and functionality *in vivo*. The results indicated that the $ScCO_2$-DFA showed higher biocompatibility, enhanced chemotactic migration of endothelial progenitor cells, lower risk of vasculopathy, lower inflammatory and splenic immune responses, and better physiological-like tension responses after xenotransplantation (XTP) in ACI/NKyo rats compared with the results obtained after XTP using detergent decellularized vascular grafts (SDS-DFA). In conclusion, $ScCO_2$ is an excellent decellularization technique in the fabrication of biocompatible vascular grafts and has tremendous application in vascular regenerative medicine.

Received 5th August 2022,
Accepted 1st February 2023

DOI: 10.1039/d2bm01233b

rsc.li/biomaterials-science

1. Introduction

Synthetic vascular grafts used in humans are associated with a lower rate of primary patency and an increased rate of infection of arteriovenous fistulas. Higher rates of thrombosis and infection are observed after the use of common synthetic vascular grafts such as Dacron and expanded polytetrafluoroethylene (PTFE). These complications are clinically unsatisfactory.[1] An emerging strategy that shows great promise is the use of tissue engineering to produce innovative vascular grafts for clinical translation.[2,3] Decellularized blood vessels possess an extracellular matrix and structural architecture comparable to that of native blood vessels, but induce a significantly decreased level of immune response.[4] Animal studies using decellularized blood vessels have shown encouraging results,[5] and therefore, the results were extrapolated to humans. Bioengineered human acellular vessels for dialysis access have recently been used in human clinical trials.[6] Detergent decellularized heterologous rat carotid arteries developed using a rodent arteriovenous graft model showed good patency in a

[a]*Graduate Institute of Medical Sciences, National Defense Medical Center, Taipei, Taiwan*
[b]*Division of Cardiovascular Surgery, Department of Surgery, Tri-Service General Hospital, National Defense Medical Center, Taipei, Taiwan*
[c]*Institute of Oral Biology, National Yang-Ming Chiao-Tung University, Taipei, Taiwan*
[d]*Department and Graduate Institute of Pharmacology, National Defense Medical Center, Taipei, Taiwan*
[e]*R&D Center, ACRO Biomedical Co. Ltd, Kaoshiung, Taiwan*
[f]*Institute for Structural Biology, Drug Discovery and Development, Virginia Commonwealth University, Virginia, USA*
[g]*Taipei Heart Institute, Taipei Medical University, Taipei, Taiwan. E-mail: g870905@tmu.edu.tw, sung1500@mail.ndmctsgh.edu.tw, cvsallen@mail.ndmctsgh.edu.tw*
[h]*Division of Cardiology and Cardiovascular Research Center, Taipei Medical University Hospital, Taipei, Taiwan*
[i]*Department of Internal Medicine, College of Medicine, School of Medicine, Taipei Medical University, Taipei, Taiwan*

small animal model, comparable to the results obtained with control autologous carotid artery grafts.[7,8] The decellularized artery conserves the structure and mechanical properties of the blood vessels without immunological reactivity.

Indeed, decellularized vascular tissue derivatives of allogenic or xenogenic nature are potential sources for the development of artificial vascular conduits, which would resolve the problems of donor vessel shortage and adverse immune issues in the recipient. Currently, the decellularized vascular grafts that are available for clinical use are Artegraft® (bovine carotid artery), Solcograft (bovine carotid artery), ProCol® (bovine mesenteric vein), and SynerGraft® (bovine ureter).[9,10] Vascular grafts are also used for vascular access during hemodialysis. In the case of peripheral bypass surgery, large-diameter grafts are required. Nowadays, decellularized xenogenic grafts provide superior outcomes than alternative synthetic conduits.

Decellularization is performed by subjecting tissues to freeze–thaw cycles, osmotic gradients, solvents, detergents, enzymes, chelating agents, and various physical methods.[11] In the case of vascular tissues, high hydrostatic pressure is used for decellularization.[12,13] During decellularization, the cells of the tissue that is being processed are completely removed. Decellularized scaffolds contain an extracellular matrix, which is meant to retain the mechanical properties of natural vessels like withstanding changes in blood pressure, encouraging tissue remodeling and regeneration, and offering a platform for numerous cell signaling molecules that are indispensable for cellular processes such as vascular cell adhesion, migration, proliferation, and differentiation.[14] However, in practice, the results are unsatisfactory; in preliminary studies where SynerGraft® was used, enhanced risk of aneurysm, poor long-term patency, high infection rates, development of graft-related thrombosis, and inflammatory response were observed.[15,16] In addition to poor performance, the other disadvantage of decellularized vascular grafts is their exorbitant price compared with the cost of synthetic grafts, because of which they are not widely used in clinics.[14] Therefore, it is necessary to devise an efficient, cheap graft that can meet the needs of various vascular troubles in clinical patients. At present, four types of techniques are used for decellularization: chemical, biological, physical, and a combination of any two or all three of these methods. Regardless of the technology used to construct decellularized biological scaffolds, the ultimate goal is to remove antigens from the donor graft, reduce allograft rejection in the recipient, and reserve the extracellular matrix of the tissue to provide a scaffold where the recipient's cells can attach and differentiate. However, grafts prepared using these methods often have defects and exhibit adverse reactions in clinical applications. To date, scientists do not know why these defects originate, and factors such as chemical damage and presence of detergent residues are highly suspected.[17]

Supercritical carbon dioxide ($ScCO_2$) has been used in decellularization technologies in recent years. $ScCO_2$ is CO_2 whose temperature and pressure are maintained at or increased beyond its critical temperature (31.1 °C) and critical pressure (7.38 MPa). In the supercritical state, CO_2 is present in a fluid phase with properties of both liquid and gas. It is an inert, non-toxic, residue-free, nonflammable, and nonexplosive solvent.[18,19] In 2020, Schmidt *et al*. discovered that $ScCO_2$ can be used for the process of decellularization, and is beneficial for the long-term preservation of tissues.[20] After transplantation, the recipient's own hematopoietic stem cells migrate to the scaffold and regenerate new blood vessels, which in theory can effectively reduce thrombosis and increase the patency rate, comparable to their own blood vessels. We have previously reported that $ScCO_2$-produced acellular porcine corneas show excellent biocompatibility following lamellar corneal transplantation in rabbits.[21] Since the products (graft or scaffold) produced by decellularization using $ScCO_2$ show high biocompatibility, we wanted to use this method to fabricate vascular grafts and analyze their efficacy, parameters regarding rejection by the recipient's immune system and biocompatibility, structural regeneration, and functionality *in vivo*. In this study, we developed a vascular graft that meets clinical requirements and is economically beneficial as well.

2. Materials and methods

2.1. Authorization of animal studies

All animals were handled according to protocols approved by the Institutional Animal Care Committee of the National Defense Medical Center (IACUC-19-195). The procedures followed regarding the treatment of animals complied with the "Guide for the Care and Use of Laboratory Animals" published by the U.S. National Institutes of Health (NIH Publication No. 85-23, revised 1996).

2.2. Preparation of the supercritical CO_2-decellularized femoral graft ($ScCO_2$-DFA) and sodium dodecyl sulfate-decellularized femoral graft (SDS-DFA) from rabbit tissue

Arterial grafts were harvested from 6-month-old male New Zealand white rabbits (weighing approximately 3 kg). Briefly, the rabbits were anesthetized and the hair on their belly and groin was shaved. The femoral artery was harvested and disinfected using Provo-iodine and 80% ethanol, followed by a midline abdominal incision. Decellularization of rabbit femoral arteries was performed using supercritical CO_2 extraction technology, as described previously.[22,23] The saline-washed rabbit femoral arteries were placed in a supercritical vessel containing 75% alcohol. The supercritical system was incubated under pressure and temperature conditions of 25–35 MPa and 30–35 °C, respectively, for 90 min. In addition to the $ScCO_2$-DFA, chemically decellularized scaffolds were produced using detergents, as described in a previous report.[24] In short, rabbit femoral arteries were soaked in a mixture of 0.5% sodium dodecyl sulfate (SDS) and 0.5% sodium deoxycholate (SDC) for 72 h, followed by washing with phosphate buffered saline (PBS) containing antibiotics for 6 days. Subsequently, the decellularized scaffolds that were produced were placed in PBS containing antibiotics at 4 °C for future use.

2.3. Characterization of the decellularized artery graft

2.3.1. Hematoxylin and eosin staining. The decellularized graft was fixed using 4% paraformaldehyde followed by paraffin embedding. The graft was cut into 5 μm-thin sections and stained with hematoxylin and eosin (HE) to confirm that the tissue was completely decellularized. The decellularized tissues were photographed and analyzed using a light microscope.

2.3.2. DNA quantification. The efficiency of supercritical CO_2 decellularization was determined by electrophoresing the genomic DNA that was extracted from the arteries (decellularized graft and non-decellularized femoral artery) using the Easy Pure Genomic DNA Mini Kit (Bioman, Taipei, Taiwan). A portion of the extracted genomic DNA was cleaved using EcoRI. Then, the digested and undigested genomic DNA samples were subjected to agarose gel electrophoresis.

2.4. Grouping and procedure of the animal study

2.4.1. Orthotopic aortic transplantation (OAT) and xeno-transplantation (XTP). PVG/Seac (donor rats) and ACI/NKyo (recipient rats) rats were purchased from the National BioResource Project (NBRP rat no. 0001), Kyoto, Japan. In this study, 8-week-old male ACI/NKyo rats (250–300 g body weight [BW]) were used as transplant recipients. We transplanted a PVG/Seac rat thoracic aorta into the ACI/NKyo rat abdominal aorta as a positive control for vasculopathy (allograft vasculopathy). The allograft OAT procedure has been demonstrated in a previous study.[25] For XTP, approximately 1 cm of the $ScCO_2$-DFA or SDS-DFA was anatomized with 7-O silk sutures onto the abdominal aorta of ACI/NKyo rats. The OAT and XTP procedures were completed within 80 min. Appropriate analgesics and antibiotics were administered three days after the surgery.

2.4.2. Animal grouping. Rats were kept in microisolator cages maintained on a 12 h day/night cycle and fed a regular rodent chow diet (scientific diet). Group 1 (ACI/NKyo sham control) consisted of sham-operated ACI/NKyo rats (which had not undergone transplantation). Group 2 ($ScCO_2$-DFA XTP) consisted of ACI/NKyo rats that had received $ScCO_2$-DFA XTP. Group 3 (PVG/Seac TA OAT, positive control of vasculopathy) consisted of ACI/NKyo rats, in which the thoracic aorta of PVG/Seac rats had been transplanted using the OAT procedure. Group 4 (SDS-DFA XTP) consisted of ACI/NKyo rats that had received SDS-DFA XTP. The rats were euthanized, and the transplanted grafts or aortas were removed at the end of the experiment (on day 30, 60, or 90).

2.5. Doppler ultrasonography

Abdominal aortic Doppler ultrasonography was performed using an ultrasound imaging system (CX50; Philips, CA, USA) with a C8-5 broadband compact linear array transducer. Mice were anesthetized using 100% oxygen mixed with 2% isoflurane in an induction chamber before being fully anesthetized. The animals were kept supine on a platform (that was heated at 37 °C) and maintained in the anesthetized state by delivery of 1.0% isoflurane through a nose cone, and their abdominal hair was removed using depilatory cream. While Doppler ultrasonography was being performed, the heart rate was continuously monitored to confirm that it was maintained at >350 beats per min. Data on blood flow parameters and aortic diameter were also collected. Doppler ultrasonography was performed before the start of the experiment (baseline), on the day after surgery, and at the end of experiment on days 30, 60, and 90.

2.6. Morphological analysis

On the 30^{th}, 60^{th}, or 90^{th} day of the experiment, animals were anesthetized and euthanized. The transplanted graft and spleen were then harvested, gently dissected free of adherent tissues, rinsed with ice-cold PBS, immersed and fixed in 4% buffered paraformaldehyde, embedded in paraffin, and cross-sectioned for HE, immunohistochemical, and immunofluorescent staining. The spleens were weighed before fixation with paraformaldehyde. Grafts were also collected and stained with picrosirius red to identify collagen fibers and visualize collagen accumulation. Immunohistochemical analysis of the graft was performed using anti-SMA (Santa Cruz Biotechnology, Dallas, TX, USA; IHC 1 : 100), anti-CD4 (Abcam Inc., Cambridge, MA, USA), anti-CD8 (Abcam Inc., Cambridge, MA, USA), anti-CD11b (Abcam Inc., Cambridge, MA, USA), anti-vWF (Chemicon International, Carlsbad, CA, USA), and anti-S100A4 (Cell Signaling Technologies, Danvers, MA, USA) antibodies, and examination of the spleen was performed using anti-CD4, anti-CD8, anti-CD11b, anti-CD20 (Abcam, Cambridge, MA, USA), and anti-CD138 (Invitrogen, Thermo Fisher Scientific Co., Carlsbad, CA, USA) antibodies, followed by the use of 3,3′-diaminobenzidine (DAB)/hydrogen peroxide in Tris-HCl buffer as a chromogen. Immunofluorescent staining of the graft was performed using Alexa 488-conjugated anti-CD133 (Bioss Antibodies Inc., Woburn, MA, USA) and Cy5-conjugated anti-CD34 (Bioss Antibodies Inc., Woburn, MA, USA) antibodies, followed by staining with the fluorescent dye 2′-[4-ethoxyphenyl]-5-[4-methyl-1-piperazinyl]-2,5′-bi-1H-benzimidazole trihydrochloride trihydrate (Hoechst 33342; Invitrogen, Carlsbad, CA, USA) to visualize cellular nuclei. The slides were observed using light microscopy or fluorescent confocal microscopy.

The coverage of vascular endothelial cells was estimated from the results of vWF staining. The graft was cross-sectioned every 5 μm from the middle to the anastomotic end and 10 consecutive slices were performed; all tissue slides were subjected to vWF staining and DAB coloring, and then the sum of endothelial cells present in the slides was calculated with a microscope at 400 magnification. The calculation formula: coverage (cell numbers in 0.1 mm^2) = total number of cells in 10 slides × (100 000/50 × endothelium length)/(100 000/50 × endothelium length).

2.7. Graft tension assessment

The procedure for the assessment of graft tension was demonstrated in a previous report.[26] At 90 days after graft transplantation, the rats were euthanized, and grafts were obtained and

cleared of adhering periadventitial fat. Then 2 mm of the graft ring was cut and mounted in the bath chamber of a wire myograph (Multi Wire Myograph System-Model 620 M, Danish Myo Technology, Aarhus, Denmark) filled with Krebs' solution and incubated under oxygenated conditions (95% O_2 plus 5% CO_2) at 37 °C for 1 h to maintain basal tension. The graft contractile response was examined by treatment with phenylephrine (PE, 1–10 μM). The relaxation response was assayed by administration of acetylcholine (Ach, 1–10 μM) in the graft rings that were pre-contracted with phenylephrine. Ach-induced relaxation was expressed as the percentage decrease in the PE-induced tone.

2.8. Liquid chromatography-tandem mass spectrometry (LC-MS)

Femoral arteries were harvested from New Zealand White rabbits. Three femoral arteries were decellularized using the $ScCO_2$ technique and three femoral arteries were decellularized using SDS-SDC detergents. Total protein was extracted from the decellularized graft. Protein samples were digested using the filter-aided sample preparation (FASP) method to generate tryptic peptides for LC-MS analysis. In brief, the samples were buffer exchanged with a molecular weight cut-off filter (Microcon YM-30; Merck Millipore Inc., Temecula, CA, USA), and the proteins were digested on the membrane by adding trypsin. All the digested peptides were collected and dried in a vacuum centrifuge tube. Prior to LC-MS analysis, all dried peptide mixtures were dissolved in 0.1% trifluoroacetic acid and desalted. LC-MS analysis was performed using a nanoACQUITY UPLC System (Waters Corporation, Milford, MA, USA) coupled with a high-resolution mass spectrometer (Thermo Fisher Scientific, Waltham, MA, USA). The mass spectrometer was operated in data-dependent mode with the following acquisition cycle: a full scan (m/z 350–1600) was recorded using an orbitrap analyzer at a resolution (R) of 240 000, and 10 peaks showing the maximum intensity and charge ≥2 were selected and fragmented using CID at a normalized collision energy of 35.

2.9. Statistical analyses

Values are expressed as mean ± SD. Non-parametric ANOVA, followed by the Kruskal–Wallis test, was used for statistical analyses. Statistical significance was set at $p < 0.05$.

3. Results

3.1. $ScCO_2$ and SDS-SDC detergents could remove the cellular contents completely and no residual DNA was left in rabbit femoral arteries

To confirm the decellularization efficiency of $ScCO_2$ and SDS-SDC detergents and to confirm that the vascular scaffolds had intact structures but no cellular content, we performed HE and Sirius red staining on the vascular scaffolds. In addition, we performed genomic DNA electrophoresis of the scaffolds to detect residual DNA. Fig. 1A shows that the rabbit femoral artery, which was not decellularized (non-DFA), had a complete vascular structure, and many nuclei in the vessel wall were stained with eosin. The vessels decellularized with $ScCO_2$ and SDS-SDC no longer exhibited nuclei in the vessel wall. Sirius red-stained slides also showed that the non-DFA grafts had uniform and evenly distributed collagens (green, yellow, and orange) in the vessel wall. In the $ScCO_2$-DFA and SDS-DFA grafts, the distribution and arrangement of collagen were like those in non-DFA grafts. However, when the $ScCO_2$-DFA was compared with the SDS-DFA, the SDS-DFA showed relatively sparse collagen in the vessel wall. Additionally, genomic DNA electrophoresis showed that a large amount of genomic DNA was present in the non-DFA group (lanes showing undigested and EcoRI-digested genomic DNA in Fig. 1B). However, the $ScCO_2$-DFA and SDS-DFA groups had almost no residual DNA left in the vessel wall. These results indicated that $ScCO_2$ and SDS-SDC detergents effectively removed the cellular contents of the femoral artery while maintaining its structural integrity, although the structure of the SDS-DFA is loose compared with that of the $ScCO_2$-DFA. The residual DNA left in the vessel wall was also confirmed using spectrophotometry (Fig. 1C).

3.2. $ScCO_2$-DFA exhibits physiological-like vessel regeneration in XTP rats

To examine the functional and structural changes in the $ScCO_2$-DFA and SDS-DFA after XTP of ACI/NKyo rats, we measured the diameter and blood velocity of the grafted $ScCO_2$-DFA and SDS-DFA during the experimental period using Doppler ultrasonography. Photographs (shown in the upper row of Fig. 2A) revealed that both the $ScCO_2$-DFA and SDS-DFA were anastomosed (black arrows) to the abdominal aorta (white arrows) of ACI/NKyo rats. At 60 and 90 days after $ScCO_2$-DFA XTP, there was no swelling or deformation of the grafts and no aneurysms were found in ACI/NKyo rats by Doppler ultrasonography (the lower row, white arrows). However, although the SDS-DFA was completely anastomosed to the abdominal aorta, graft enlargement and deformation (upper row, white arrowheads) appeared after 90 days of XTP, and Doppler ultrasonography also showed enlarged vessels (the lower row, white arrows) in ACI/NKyo rats. Calculations were performed using the values obtained from the measurement of parameters (vessel diameter and blood flow velocity) of all ACI/NKyo rats by Doppler ultrasonography and are presented in Fig. 2B and C. The results showed that the luminal diameter of the $ScCO_2$-DFAs was constantly maintained until the ACI/NKyo rats were euthanized on day 90 post-XTP (diameter on day 1 post-XTP: 1.49 ± 0.11 mm; day 90 post-XTP: 1.54 ± 0.14 mm), while the SDS-DFAs showed a significant increase in the luminal diameter of the vessel (day 1 post-XTP: 1.42 ± 0.12 mm; day 90 post-XTP: 4.2 ± 0.61 mm; Fig. 2B). There was no significant change in blood velocity in any of the groups (Fig. 2C). Additionally, to examine the systolic and diastolic capacity of the ScCO2-DFA and SDS-DFA after XTP, the grafts were removed after the rats were euthanized and the graft tension was assessed. Interestingly, PE induced dose-dependent vasocontraction was observed in the $ScCO_2$-DFA rings,

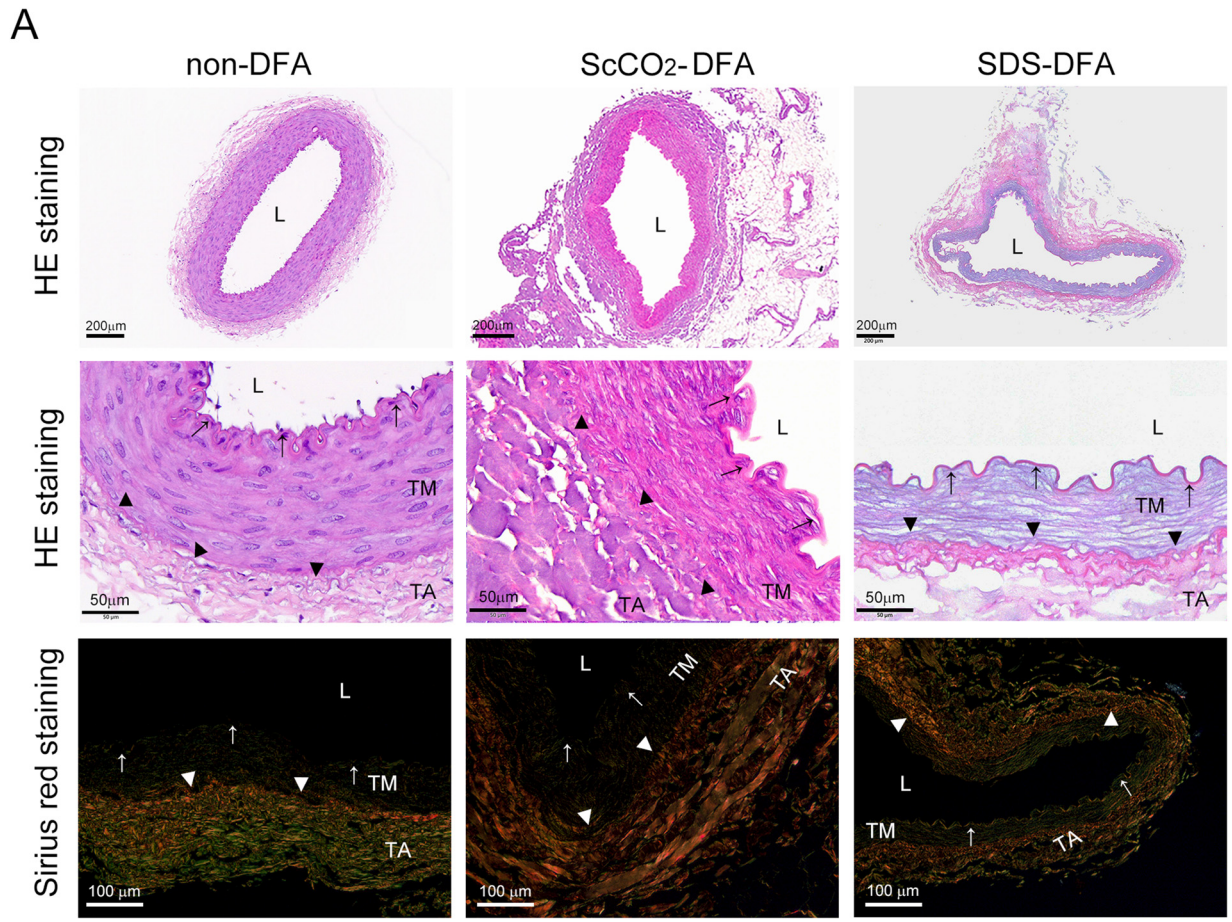

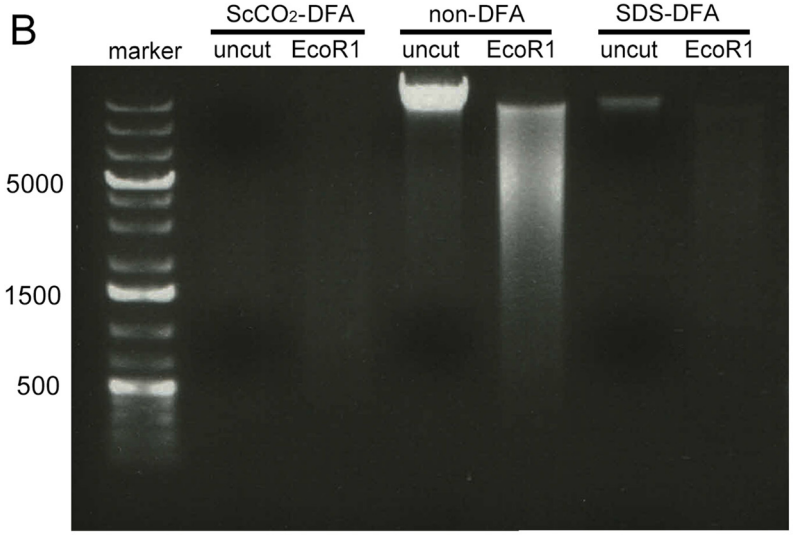

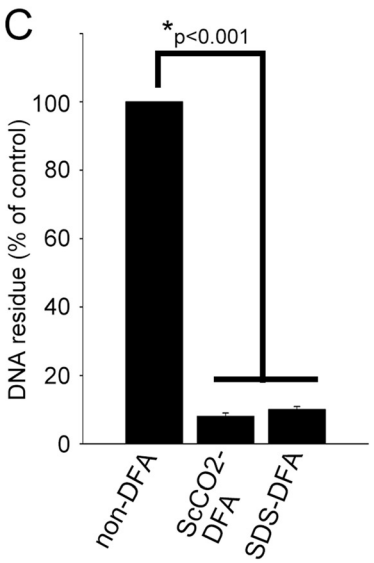

Fig. 1 $ScCO_2$ and SDS-SDC detergents can effectively remove the cellular contents of the rabbit femoral artery and preserve the intact structure of the vessel wall. (A) Sections of femoral arteries from rabbits stained with hematoxylin and eosin. The slides were observed *via* light microscopy (the upper row was visualized in 40× magnification and the middle row was 400× magnified). The distribution and integrity of collagen on the arteries were observed by picrosirius red staining (the lower row) and polarized light microscopy at 200× magnification. The vessel lumen (L), tunica media (TM), tunica adventitia (TA), internal elastic laminae (arrows), and external elastic laminae (triangles) were identified. (B) Genomic DNA extracted from the non-DFA, $ScCO_2$-DFA, and SDS-DFA were electrophoresed. A part of the extracted genomic DNA was digested using EcoRI. Then the undigested and digested genomic DNA were electrophoresed on agarose gel. (C) The residues of genomic DNA in the vessel were identified using spectrophotometry and then the DNA was extracted. The results are expressed as the mean ± SD. Statistical significance was set at $p < 0.05$.

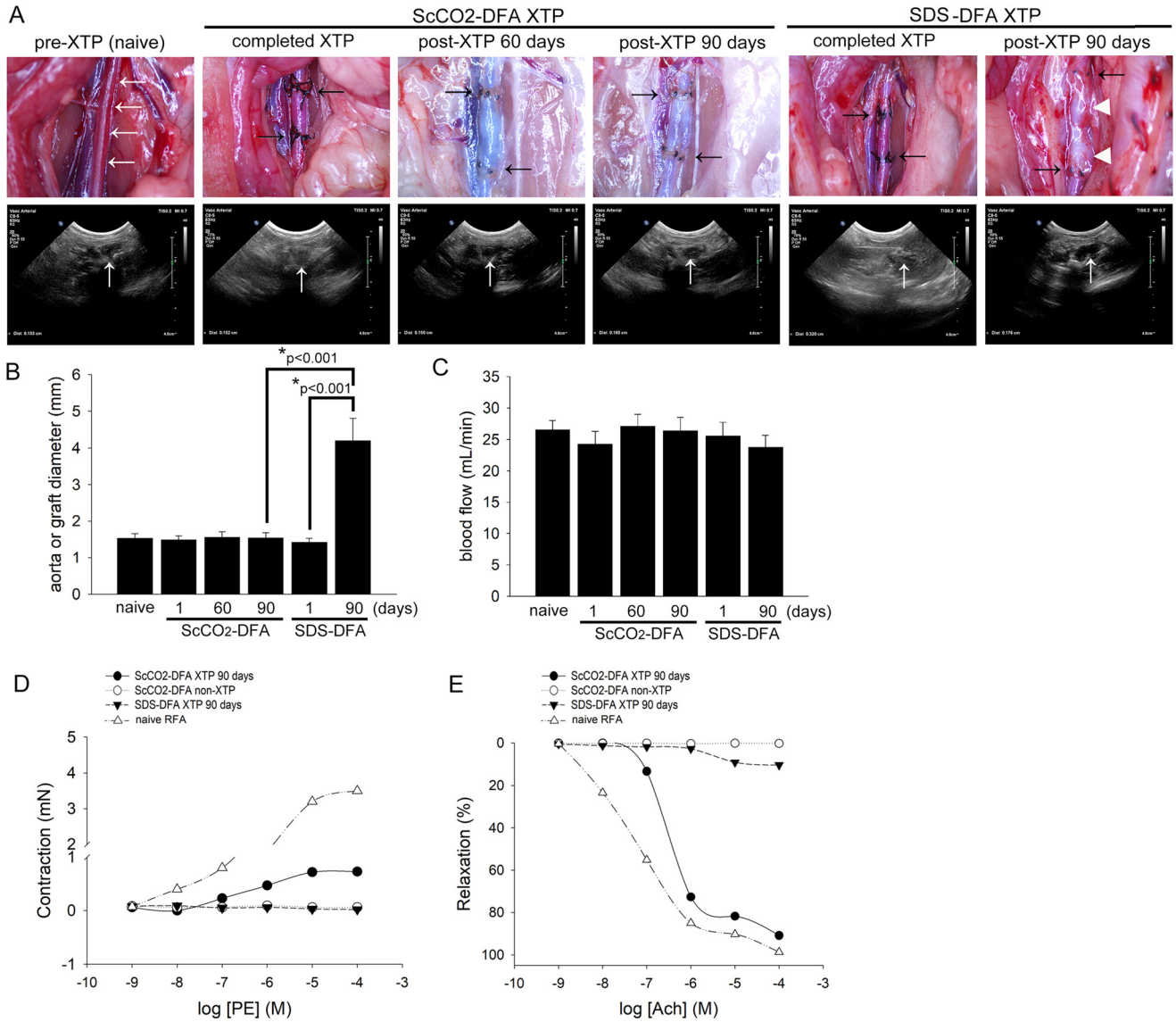

Fig. 2 $ScCO_2$-DFA maintains the normal vascular structure and leads to physiological-like vessel regeneration in XTP rats. (A) Upper row, photographs show the appearance of the abdominal aorta in a naïve ACI/NKyo rat (white arrows), complete anastomosis (black arrows) of scaffolds ($ScCO_2$-DFA and SDS-DFA) on days 60 and 90 after XTP. The white arrowheads indicate the aneurysmal change in the scaffold. The lower row shows pictures of the abdominal aorta analyzed by Doppler ultrasonography. The white arrows indicate the location of abdominal aorta. (B and C) Aorta graft/scaffold diameter and blood velocity measured *via* Doppler ultrasonography are respectively depicted in the bar graph. The results are expressed as the mean ± SD. Statistical significance was set at $p < 0.05$. (D and E) Concentration–response curves showing the effect of phenylephrine (PE) and acetylcholine (Ach) treatment on the naïve rabbit femoral artery (naïve RFA), $ScCO_2$-DFA and SDS-DFA, respectively. A graft ring showing response to the PE and Ach is depicted in the graphs.

but not in the SDS-DFA rings in ACI/NKyo rats that underwent XTP (XTP ACI/NKyo rats) and in the $ScCO_2$-DFA rings in ACI/NKyo rats that did not undergo XTP (non-XTP $ScCO_2$-DFA rings; Fig. 2D). Moreover, the $ScCO_2$-DFA rings in XTP ACI/NKyo rats showed vasodilation after stimulation by Ach. In contrast, vasodilation response was absent in the SDS-DFA rings in XTP ACI/NKyo rats and in the non-XTP $ScCO_2$-DFA rings (Fig. 2E). In addition, Fig. 2D and E showed that the pattern of contraction and relaxation of the SCO_2-DFA XTP ring was similar to that of the naive rabbit femoral artery (naive RFA) ring, although its strength was significantly weaker than that of the naive RFA. These results indicated that the ScCO2-DFA offered physiological-like conditions for vessel regeneration, with contractions and dilations that resembled those in naïve vessels. Similar results were not obtained using the SDS-DFA for XTP in rats.

3.3. Low risk of aneurysm and vasculopathy is observed after XTP using the $ScCO_2$-DFA in rats

Aneurysmal changes and vasculopathy of vascular scaffolds caused by inflammation after implantation are some of the main problems encountered in current clinical applications.

Therefore, we used immunohistochemical assays to analyze pathological changes in the $ScCO_2$-DFA and SDS-DFA after XTP in ACI/NKyo rats. As shown in Fig. 3A, the abdominal aorta of naïve ACI/NKyo rats had an intact vascular wall structure (HE staining), and the pattern of orientation of collagen fibers corresponded to the type of collagen fiber that was observed (Sirius red staining). The PVG/Seac TA rats survived severe vasculopathy after 90 days of OAT, but showed calcified plaque formation (black arrows) and abnormal accumulation of collagen (white rectangle) in the vessel wall. The SDS-DFA showed significant aneurysmal changes (black rectangle), and there was abnormal accumulation of collagen in the vascular wall after 90 days of XTP. In contrast, compared with the PVG/Seac TA-OAT and SDS-DFA, the ScCO2-DFA after 90 days of XTP did not show calculated plaques, aneurysms. Additionally, there were no aberrations in the type and arrangement of collagen fibers. The distribution of muscle cells and fibroblasts on the vessel wall affects arterial function; therefore, we examined the distribution of these two types of cells in the scaffold 90 days after XTP. Fig. 3B shows that in naïve ACI/NKyo abdominal aorta, vascular smooth muscle cells (αSMA-positive cells) were mainly distributed in the tunica media of the artery and oriented parallel to the vessels, and exhibited directionality; some fibroblasts (S100A4-positive cells) were also distributed in the media of the artery. The graft in the PVG/Seac TA group showed a disorderly pattern of distribution of vascular smooth

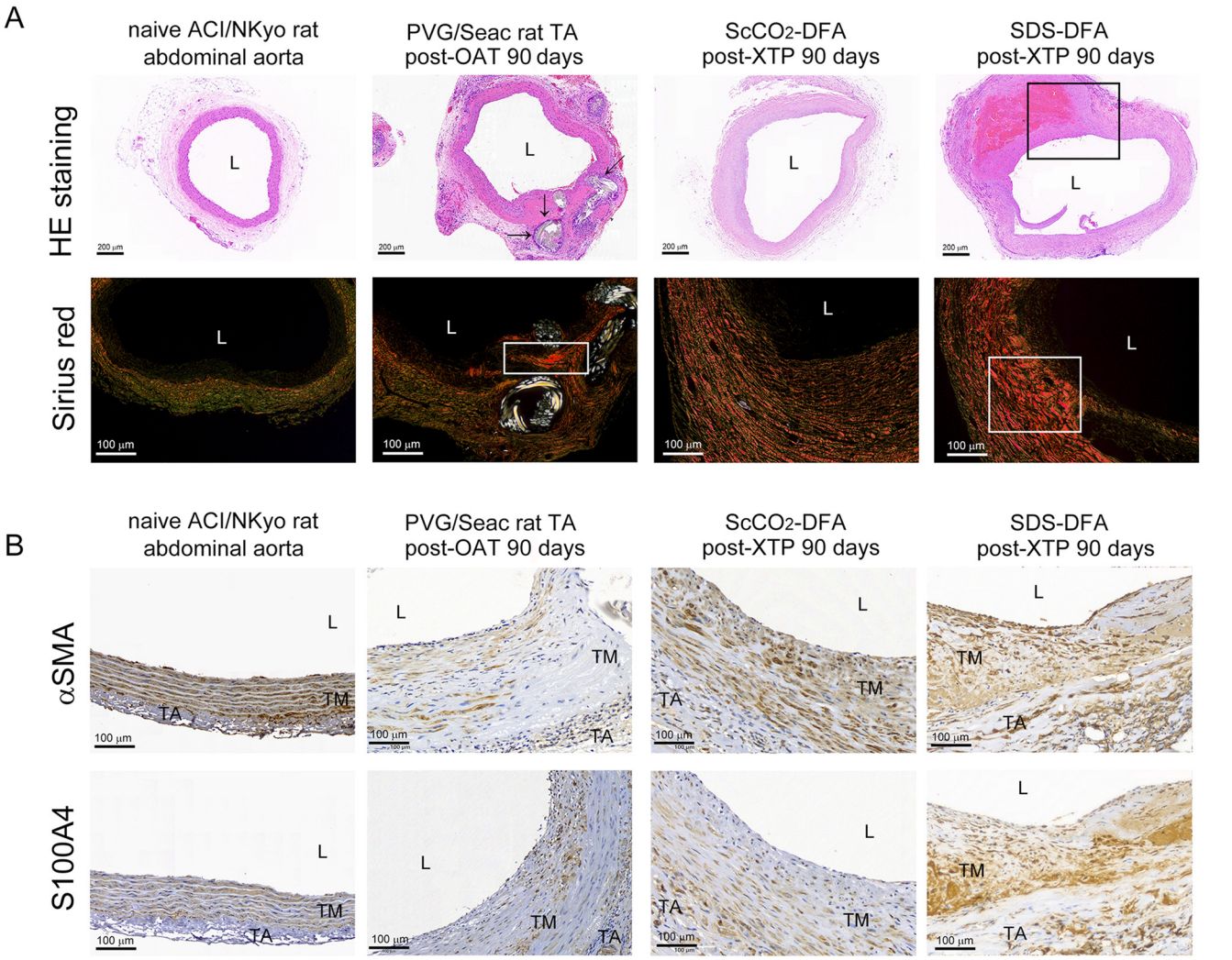

Fig. 3 $ScCO_2$-DFA leads to low risk of aneurysmal change and vasculopathy in XTP rats. (A) Upper row, the naïve ACI/NKyo rat abdominal artery, $ScCO_2$-DFA and SDS-DFA in recipient ACI/NKyo rats on day 90 post-XTP, and the PVG/Seac rat thoracic artery in recipient ACI/NKyo rats on day 90 post-OAT, stained with hematoxylin and eosin. The black arrows indicate calcified lesions and the black rectangular box indicates the aneurysmal change. The slides were observed *via* light microscopy at 40× magnification. Lower row, collagen accumulation and pathological features of the thoracic aorta were observed using picrosirius red staining. The uppermost part in all sections represents the lumen. The slides were observed *via* polarized light microscopy at 200× magnification. (B) Immunohistochemical analysis to identify proliferated SMCs (αSMA^+ cells) and fibroblasts ($S100A4^+$ cells). They were identified by the brown-color signals received from the naïve aorta and from the transplanted scaffolds/grafts present in recipient ACI/NKyo rats. The vessel lumen (L) was identified.

muscle cells and fibroblasts on day 90 post-OAT. In the SDS-DFA group, many vascular smooth muscle cells and fibroblasts accumulated in the tunica media of the XTP scaffold on day 90 post-XTP, and were greater than those observed in PVG/Seac TA rats after 90 days of OAT. On the basis of these results, we concluded that aneurysmal changes and vasculopathy following the $ScCO_2$-DFA were less pronounced than the changes observed in the SDS-DFA in XTP rats.

3.4. $ScCO_2$-DFA induces a diminished immune response in the vascular scaffold and spleen after XTP in ACI/NKyo rats

Activation of immune cells and their subsequent accumulation in the vascular scaffold are critical phenomena in the inflammatory response. Therefore, immunohistochemical staining was performed to detect $CD4^+$T (helper) cells, $CD8^+$T (cytotoxic) cells, and $CD11b^+$ macrophages in transplanted grafts. As shown in Fig. 4A, the accumulation of $CD11b^+$ macrophages, $CD4^+$T cells, and $CD8^+$T cells was not observed in the aortic walls of naïve ACI/NKyo rats. In contrast, numerous T lymphocytes and macrophages accumulated in the vessel wall in the PVG/Seac TA rats (vasculopathy control group) on day 90 post-OAT. Surprisingly, a less number of T lymphocytes and macrophages accumulated in the $ScCO_2$-DFA group post-XTP. A higher accumulation of T lymphocytes and macrophages in the scaffold was observed in the SDS-DFA group post-XTP than the level of accumulation observed in the $ScCO_2$-DFA group post-XTP. These results indicated that very few adaptive immune reactions occurred in the scaffold of the $ScCO_2$-DFA group post-XTP. Furthermore, relatively minimal adaptive immune reactions occurred in the scaffold of the SDS-DFA group post-XTP, resulting in increased infiltration of T lymphocytes and macrophages. These results showed that the ScCO2-DFA induced inflammatory response to a lesser extent in ACI/NKyo rats than the enhanced level of inflammatory response seen in the SDS-DFA XTP group. Spleen weight is associated with immune responses that originate from transplantation-related rejection. Therefore, we weighed the spleens of euthanized ACI/NKyo rats. As shown in Fig. 4C, the average weight

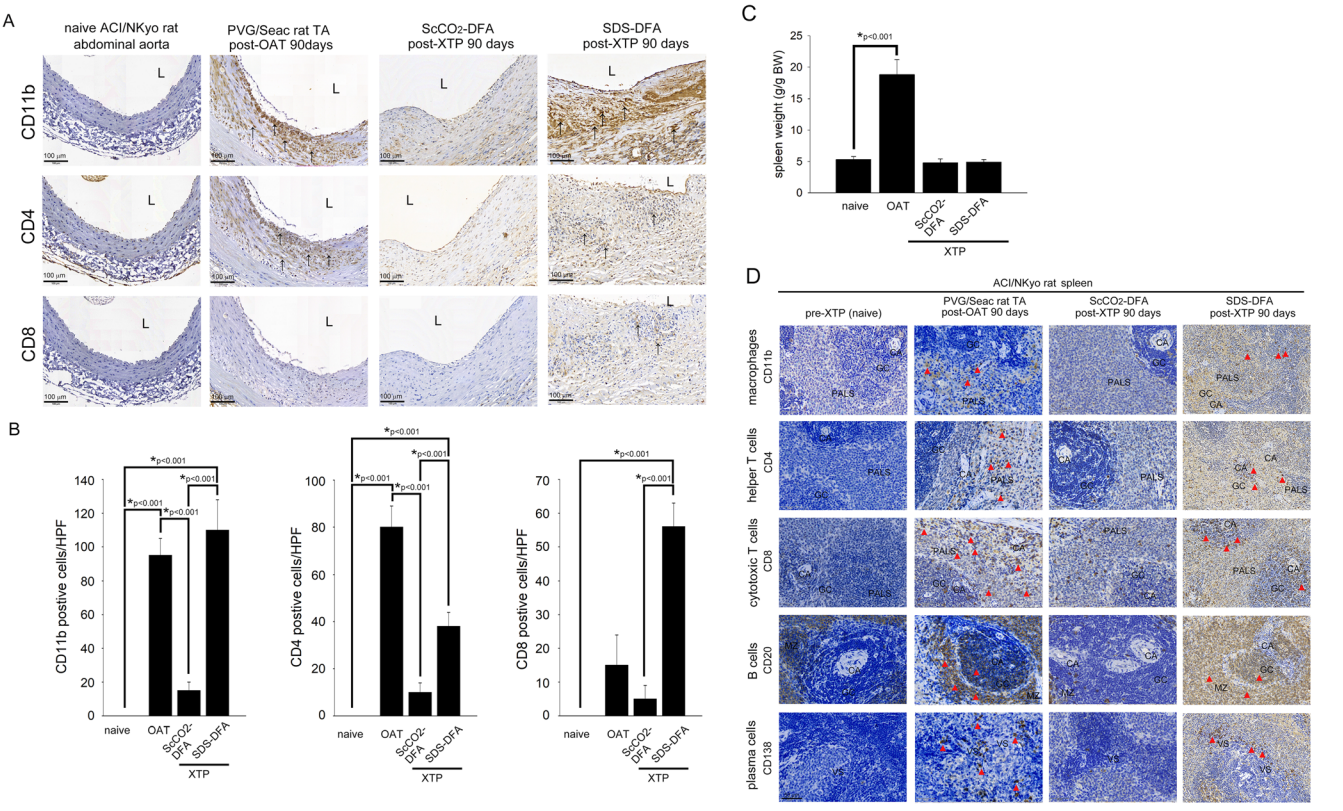

Fig. 4 $ScCO_2$-DFA induces lower levels of inflammatory and immune responses in the XTP ACI/NKyo rats. (A) Immunohistochemical analysis of accumulated and infiltrated $CD11b^+$ macrophages, $CD4^+$ helper T cells, and $CD8^+$ cytotoxic T cells in the vessel wall from naïve ACI/NKyo rats, ScCO2-DFA rats post-XTP, SDS-DFA rats post-XTP, and PVG/Seac TA rats post-OAT. The images are 200× magnified and the arrows indicate the brown-color signal received from $CD4^+$, $CD8^+$, and $CD11b^+$ cells. (B) Semi-quantification of immunohistochemically positive stained cells in a high power field (HPF) is shown. The graphs represent the accumulation of cells in the aortas of rats from the experimental groups. The results are expressed as the mean±SD. Statistical evaluations were performed using the Student t-test, followed by Dunnett's test. *$p < 0.05$ was considered as significant. The vessel lumen (L) was identified. (C) The spleens were weighed after the recipient ACI/NKyo rats were euthanized. The results were calculated and demonstrated using a bar graph showing mean body weight (BW; g per g). The bars are expressed as the mean ± SD. *Statistical significance was set at $p < 0.05$. (D) Immunohistochemistry was used to analyze the accumulation of macrophages, helper T cells, cytotoxic T cells, B cells, and plasma cells in the spleen of naïve and recipient ACI/NKyo rats (CA, central artery; PALS, periarterial lymphatic sheath; GC, germinal center; MZ, mantle zone; VS, venous sinuses). The images are 400× magnified and the red arrowheads indicate the cells.

of the spleen of naïve ACI/NKyo rats was 5.3 ± 0.5 g per g body weight (BW). The spleens of the ACI/NKyo rats, which underwent OAT surgery, were significantly heavier than those of the naïve ACI/NKyo rats (approximately 18.8 ± 2.4 g per g BW). However, there were no significant differences in the spleen weight of the $ScCO_2$-DFA XTP (4.8 ± 0.6 g per g BW) and SDS-DFA XTP (4.9 ± 0.4 g per g BW) groups, which was comparable to the spleen weight of the naïve ACI/NKyo rats. The $CD11b^+$ macrophages deliver antigens and trigger adaptive responses. Major histocompatibility complex class II (MHC class II) molecules deliver antigens to $CD4^+$T cells, and the $CD8^+$T cells regulate MHC class I-restricted interactions, which mediate adaptive immunity. $CD20^+$B cells produce antibodies and may differentiate into $CD138^+$plasma cells, which regulate the humoral immune response. Since these cells play important roles in immune response after transplantation, we examined the process of activation of these cells in the spleen by immunohistochemical analysis to determine the effects of the scaffolds on the immune and inflammatory response of the individual. In the 1st row in Fig. 4D, we have shown that macrophages were present only in the splenic periarterial lymphatic sheath (PALS) and germinal center (GC) of naïve ACI/NKyo rats. In PVG/Seac TA rats, many macrophages were observed in the PALS and GC post-OAT. Like the number of macrophages seen in pre-XTP ACI/NKyo rats, fewer macrophages were present in the spleens of ACI/NKyo rats in the $ScCO_2$-DFA XTP group. In contrast, significantly increased macrophage accumulation was observed in the splenic GC and PALS following XTP using the SDS-DFA. As shown in the 2nd and 3rd rows in Fig. 4D, accumulation of helper and cytotoxic T cells was not observed in the splenic GC and PALS in naïve ACI/NKyo rats. A significantly smaller number of helper T cells accumulated after XTP using the $ScCO_2$-DFA and SDS-DFA than the number of cells observed in PVG/Seac TA rats post-OAT. However, XTP with the $ScCO_2$-DFA and SDS-DFA induced cytotoxic T cell activation, but the cytotoxicity was less severe than that observed in PVG/Seac TA rats post-OAT. As shown in the 4th and 5th rows in Fig. 4C, $CD20^+$B cells (not $CD138^+$ plasma cells) were observed in the GC, venous sinuses (VS), and mantle zone (MZ) in the naïve group. Many $CD20^+$B cells were noticed in the MZ and GC, and $CD138^+$ plasma cells were present in the VS of the spleen of ACI/NKyo rats and PVG/Seac TA rats post-OAT. In the $ScCO_2$-DFA XTP group, not many $CD20^+$B cells were found in the MZ and GC, and hardly any $CD138^+$ plasma cells were seen in the VS. However, the SDS-DFA XTP group demonstrated a significant level of activation of $CD20^+$B cells in the MZ and GC and of $CD138^+$ plasma cells in the VS. On the basis of these results, we concluded that XTP using the $ScCO_2$-DFA did not induce adaptive or humoral immune response in the ACI/NKyo rats. XTP using the SDS-DFA induced cell-mediated and humoral immune responses in ACI/NKyo rats, although the mechanism remains unknown. We performed quantitative analysis of splenic inflammatory and immune cells as shown in Table 1.

3.5. Using LC-MS analysis and database search, it was shown that the $ScCO_2$-DFA contains a variety of proteins that interact with vascular progenitor cells

To develop an appropriate vascular scaffold, vascular cells should be able to grow, differentiate, and migrate into the vascular wall. We have shown that after using the $ScCO_2$-DFA for transplantation in animals, physiologically functional vessels developed, but appropriate vessel formation was not observed when the SDS-DFA was used for transplantation. We speculated that the $ScCO_2$-DFA contains specific factors that interact with vascular progenitor cells, either directly or through chemoattractants, in addition to the fact that it induces a low level of inflammation and reduces the extent of immune cell infiltration, which is associated with the immune response. To test this hypothesis, we performed LC-MS analysis of the $ScCO_2$-DFA and SDS-DFA samples. Proteins that were co-detected in the three DFA samples were selected. The results of LC-MS analysis demonstrated that the $ScCO_2$-DFA contained 93 kinds of peptides/proteins, and the SDS-DFA contained 49 kinds of peptides/proteins. Then, out of these proteins, we searched for those related to angiogenesis and vasculogenesis; 19 proteins from the $ScCO_2$-DFA (Table 2) and 5 proteins from the SDS-DFA (Table 3) were screened out.

CD34 is a surface marker of hematopoietic stem cells and vascular progenitor cells; we used the HDOCK server (a server used to study protein–protein interactions; **https://hdock.phys.hust.edu.cn/**) to analyze the interaction of peptide fragments (shown in Tables 1 and 2; sequences were acquired from UniProtKB; **https://www.uniprot.org/**) with rat CD34. The results

Table 1 Quantitative analysis of inflammatory and immune cells in the spleen in a high power field (400× magnification)

	Pre-XTP mean ± SD	PVG/Seac rat TA post-OAT 90 days		$ScCO_2$-DFA post-XTP 90 days			SDS-DFA post-XTP 90 days	
		mean ± SD	$^a p$	mean ± SD	$^a p$	$^b p$	mean ± SD	$^a p$
Macrophages (CD11b)	5.2 ± 2.1	56.1 ± 20.8	<0.001	10.8 ± 4.5	0.934	<0.001	68.1 ± 21.2	<0.001
Helper T cells (CD4)	6.3 ± 2.4	98.5 ± 40.9	0.016	13.9 ± 6.4	0.992	0.006	120.4 ± 74.3	0.003
Cytotoxic T cells (CD8)	8.1 ± 2.2	167.3 ± 52.4	<0.001	10.2 ± 7.3	1.000	<0.001	221.9 ± 40.5	<0.001
B cells (CD20)	9.5 ± 3.1	224.9 ± 60.2	<0.001	12.8 ± 8.4	0.999	<0.001	287.8 ± 57.7	<0.001
Plasma cells (CD138)	2.2 ± 1.0	56.7 ± 10.7	<0.001	5.9 ± 3.2	0.814	<0.001	46.2 ± 7.1	<0.001

Values are represented as mean±SD. $^a p$ value compared with pre-XTP of the same cell marker. $^b p$ value compared with the SDS-DFA group post-XTP 90 days of the same cell marker; statistical evaluations were performed using one-way ANOVA and significance was set at $p < 0.05$.

Table 2 Proteins in the $ScCO_2$-DFA screened for angiogenesis and vasculogenesis

Protein	Protein entry identifier	Mnemonic identifier (UniPortKB entry)	Functions
Filamin A	B7NZP9	B7NZP9_RABIT	Homing, adhesion, migration, matrix interaction
Myosin-11	P35748	MYH11_RABIT	Migration
Myosin heavy chain 9	G1SL68	G1SL68_RABIT	Adhesion, migration,
Lamin A/C	G1SYD6	G1SYD6_RABIT	Homing, migration, differentiation
Periostin	A0A5F9C343	A0A5F9C343_RABIT	Homing
Vinculin	A0A5F9C3B7	A0A5F9C3B7_RABIT	Repopulation, homing
Integrin beta	A0A5F9C3C4	A0A5F9C3C4_RABIT	Homing, adhesion, differentiation
Sarcoglycan delta	G1SGL0	G1SGL0_RABIT	Homing
Caveolin 1	Q09YN6	CAV1_RABIT	Homing, mobilization, differentiation
Vimentin	G1SWS9	G1SWS9_RABIT	Differentiation, regeneration, homing, adhesion, migration
Desmin	B7NZH1	B7NZH1_RABIT	Differentiation, hematopoiesis
Heparan sulfate proteoglycan 2	G1TN89	G1TN89_RABIT	Homing, migration, differentiation
Spectrin alpha	G1STR7	G1STR7_RABIT	Adhesion, cell development, morphogenesis
Decorin	A0A5F9CGV4	A0A5F9CGV4_RABIT	MSC recruitment, proliferation, adhesion, migration
Talin	A0A5F9CYF1	A0A5F9CYF1_RABIT	Focal adhesion, migration
Laminin subunit beta 2	G1SN83	G1SN83_RABIT	Homing
Biglycan	U3KML1	U3KML1_RABIT	Chemoattractant
Fibrinogen gamma chain	A0A5F9CEA5	A0A5F9CEA5_RABIT	Migration
Desmoplakin	G1T4V7	G1T4V7_RABIT	Migration

Table 3 Proteins in the SDS-DFA screened for angiogenesis and vasculogenesis

Protein	Protein entry identifier	Mnemonic identifier (UniPortKB entry)	Functions
Heparan sulfate proteoglycan 2	G1TN89	G1TN89_RABIT	Homing, migration, differentiation
Decorin	A0A5F9CGV4	A0A5F9CGV4_RABIT	MSC recruitment, proliferation, adhesion, migration
Laminin subunit beta 2	G1SN83	G1SN83_RABIT	Homing
Biglycan	U3KML1	U3KML1_RABIT	Chemoattractant
Fibrinogen gamma chain	A0A5F9CEA5	A0A5F9CEA5_RABIT	Migration

showed that six peptide fragments (lamin A/C, periostin, vimentin, desmin, biglycan, and integrin β) from the $ScCO_2$-DFA interacted with rat CD34. In the SDS-DFA, only the peptide fragment of biglycan interacted with CD34 in rats. Finally, we used the UCSF Chimera program (an extensible molecular modeling system; https://www.cgl.ucsf.edu/chimera/) to visualize the interaction between the peptide fragments and CD34 (Fig. 5). On account of these results, we speculated that the decellularized vascular scaffolds prepared using $ScCO_2$ contained some elements that interacted with hematopoietic stem cells and vascular progenitor cells; however, this interaction was not observed in the vascular scaffolds prepared using SDS-SDC.

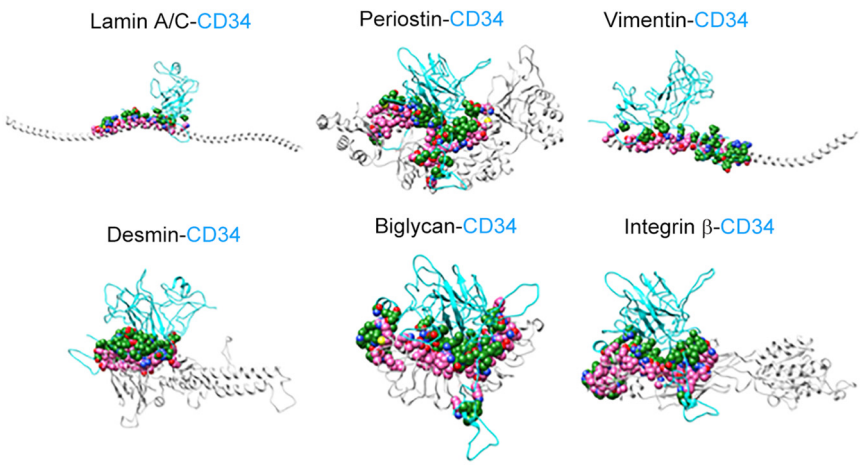

Fig. 5 Visualization of the interaction between regeneration-related peptide fragments and $CD34^+$. The UCSF Chimera program was used to reconstruct the interaction between rabbit peptide fragments and $CD34^+$ from ACI/NKyo rats.

3.6. $ScCO_2$-DFA can be used as a growth pool for $CD34^+$ vascular progenitor cells and to promote the delivery of antigens by endothelial cells

To confirm that the $ScCO_2$-DFA facilitates the chemotactic infiltration of $CD34^+$ vascular progenitor cells and enables them to develop into vascular structures similar to naïve vessels, we examined the growth and distribution of $CD34^+$ cells and endothelium formation in the transplanted DFA by immunofluorescence and immunohistochemical analyses, respectively. In Fig. 6A, analysis of $ScCO_2$-DFA XTP rats on day 30 revealed that $CD34^+$cells were evenly distributed in the vessel wall (white arrows) and did not form endothelial cells in von Willebrand factor (vWF)-stained slides; $CD34^+$ cells were observed near the vessel lumen (white arrows), although the status of vWF^+-endothelial cells remained unclear at 60 days after XTP; however, 90 days after XTP, the $CD34^+$ cells in the vessel wall disappeared and the vWF^+ endothelial cells were clearly attached to the surface of the vascular lumen (black arrows). Compared with the distribution of $CD34^+$ cells in the vessel wall of ACI/NKyo rats in the $ScCO_2$-DFA XTP group, no infiltration, growth, or distribution of $CD34^+$ cells was observed in the vessel wall on days 30, 60, and 90 after SDS-DFA XTP in ACI/NKyo rats (Fig. 6B); the formation of vWF^+-endothelial cells could not be observed by immunohistochemical analysis. Additionally, Fig. 6C shows the coverage of endothelial cells on the $ScCO_2$-DFA and SDS group at 90 days after XTP. The 90-day coverage of endothelial cells of ScCO2-DFA XTP is significantly better than that of the SDS-DFA XTP group. Therefore, these results suggested that the $ScCO_2$-DFA attached $CD34^+$ vascular progenitor cells to the vessel wall to induce endothelium formation.

4. Discussion

Due to aging of the global population, the prevalence of cardiovascular diseases, diabetes, and various metabolic diseases, and the incidence of renal failure, aneurysms, and peripheral vessel diseases are increasing every year. According to statistics from the World Health Organization, cardiovascular diseases were the leading cause of death in 2016, and a high global mortality rate of 31% (approximately 17.9 million people) was observed. Currently, autologous vessels or synthetic vascular grafts are mainly used to treat cardiovascular and peripheral vessel diseases in clinical settings. However, it is difficult to obtain suitable autologous vessels in several situations. For example, coronary artery bypass grafting is one of the most commonly used surgical procedures for the treatment of coronary heart disease, and the internal thoracic artery and great saphenous vein are widely used in this operation. Although the internal thoracic artery has a ten-year patency rate of 90%, in up to 30% of patients, the internal thoracic artery is not suitable for use after 10 years.[27,28] The ten-year patency of the great saphenous vein is only 50%, which is far less than the patency of the internal thoracic artery.[29,30] With the aging trend of the population and advancement in the field of medicine, the number of people undergoing heart reoperations is also increasing. The great saphenous vein is sometimes difficult to obtain. Therefore, the annual demand for synthetic vascular grafts is increasing.

At present, the materials commonly used for synthesizing vascular grafts are PTFE and polyester (Dacron®). Both materials have the advantage of easy availability and cost-efficiency, and their porous nature makes them highly compatible with tissues after implantation in the human body, which is a feature required by clinical patients. However, small-diameter synthetic vascular grafts made of these two materials still have shortcomings, such as a low patency rate and high rate of occurrence of thrombosis and intimal hyperplasia at the anastomotic site.[16] These phenomena are caused by the poor biological activities of PTFE and Dacron® and due to material fatigue after long-term use.[31] Therefore, the current synthetic vascular grafts are only suitable for the reconstruction of blood vessels with a diameter greater than 8 mm and are not very suitable for the reconstruction of blood vessels with a diameter less than 6 mm; that is, there is a lack of options that are available for coronary artery bypass graft surgery and pediatric cardiovascular surgery.

Natural biological vascular grafts are derived from natural blood vessels through decellularization techniques; they preserve the complete structure of the extracellular matrix and the mechanical properties of natural vascular tissue. Compared with synthetic vascular grafts, natural biological vascular grafts have better biological activity and long-term patency rates and are less prone to material fatigue after long-term use.[17] The main purpose and aim of the decellularization strategy are to remove cells and their genetic material from biological tissues to avoid immune rejection after transplantation, to retain the extracellular matrix (the main components are collagen, elastin, fibronectin, laminin, and glycosaminoglycan) to maintain the original vascular biomechanical properties[32,33] and to provide cellular signaling messages to regulate the attachment, migration, proliferation, and differentiation of regenerative cells. Many decellularization techniques are currently being developed and applied, including physical, enzymatic, and chemical treatments. However, the choice of strategy depends on the source species, organ, tissue size, and other factors.[34,35] The decellularized scaffolds produced using any of these technologies have their own advantages and disadvantages; thus, so far, no technology that is flawless has been devised for decellularization. According to previous reports, for the chemical decellularization process, among the various concentrations of detergents that have been examined, the use of 0.5% SDS + 0.5% SDC to wash small-diameter carotid arteries from hogs has been found to be the most appropriate to completely remove cellular components and preserve the original vascular structure;[24] therefore, in this study, we chose to use this method for the control group. Although reports on the analysis of biological vascular grafts prepared by using 0.5% SDS + 0.5% SDC have shown positive results, we observed the development of aneur-

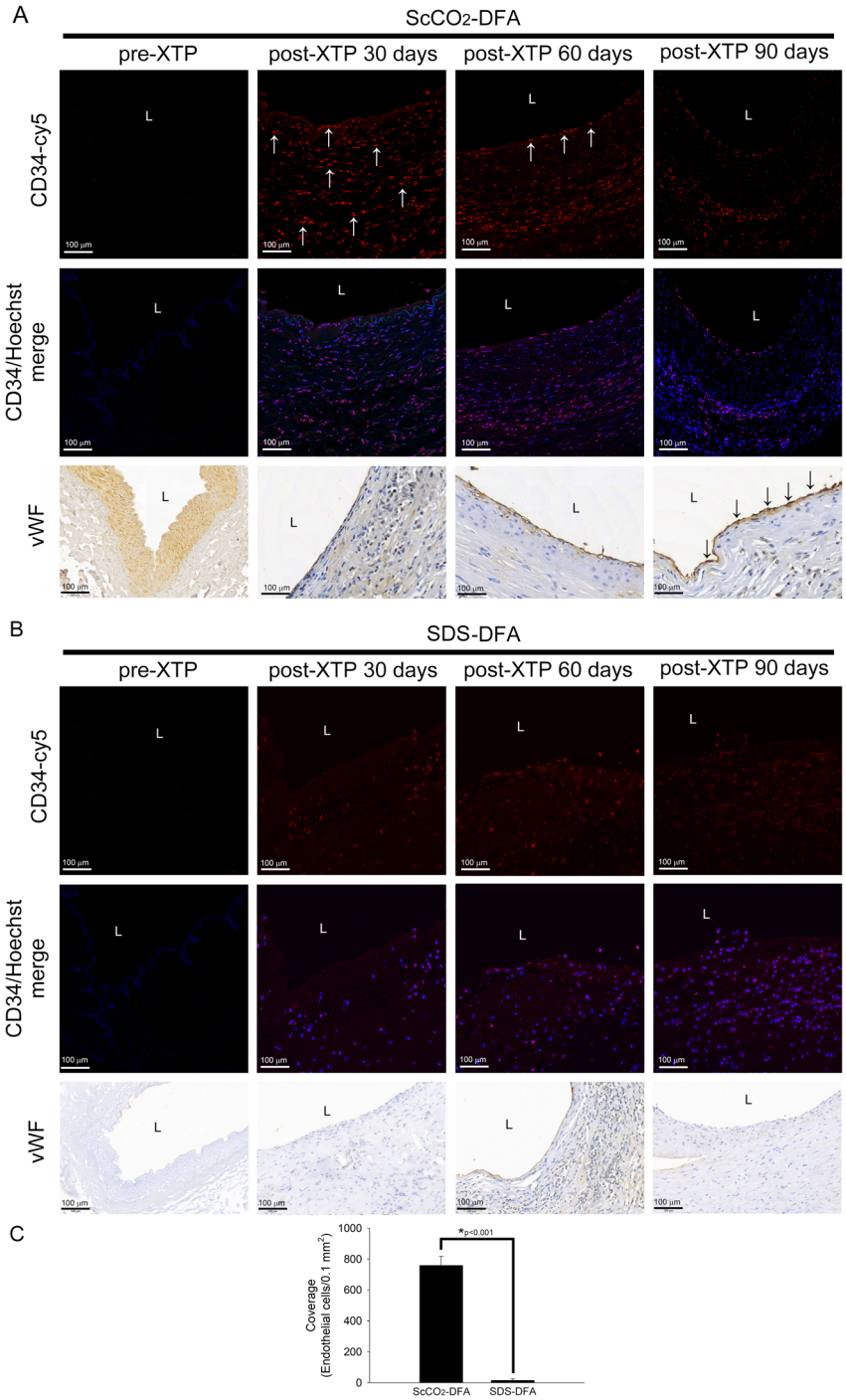

Fig. 6 $ScCO_2$-DFA attaches $CD34^+$ vascular progenitor cells to the vessel wall to induce endothelium formation. (A) Immunofluorescent and immunohistochemical analyses were used to detect $CD34^+$ vascular progenitor cells and vWF^+-endothelial cells in the pre-XTP $ScCO_2$-DFA and $ScCO_2$-DFA from ACI/NKyo rats on days 30, 60, and 90 post-XTP. The white arrows indicate $CD34^+$ vascular progenitor cells and the black arrows indicate endothelial cells. (B) The $CD34^+$ vascular progenitor cells and vWF^+-endothelial cells in the pre-XTP SDS-DFA and in SDS-DFA from ACI/NKyo rats on days 30, 60, and 90 post-XTP. The vessel lumen (L) was identified. (C) The coverage of endothelial cells in the $ScCO_2$-DFA and SDS-DFA on day 90 post-XTP was calculated by vWF staining. The bars are expressed as the mean ± SD. *Statistical significance was set at $p < 0.05$. All the fluorescent images are 200× magnified and visible light microscopic images are 400× magnified.

ysm and mild immune rejection after prolonged use (90 days post-XTP) in rats compared with the contrary results obtained from the SCO_2-DFA group.

In terms of vessel function, we also found that after vascular reconstruction, the $ScCO_2$-DFA responded to stimulation by PE and Ach. This was because the scaffold allowed specific vas-

cular cells to stay at a specific site in the vessel wall for long-term settlement. LC-MS analysis showed that after $ScCO_2$ treatment, 93 peptide fragments/proteins were present in the rabbit femoral artery, and were far greater than the number of peptides/proteins left in the DFA produced by 0.5% SDS-SDC treatment. In this study, we only analyzed peptide fragments/proteins that may interact with $CD34^+$ vascular progenitor cells in the $ScCO_2$-DFA; however, vascular regeneration is regulated by many factors, and there are many peptide fragments/proteins associated with angiogenesis and vasculogenesis that have not been analyzed (Table 2). We need to further analyze the factors present in the $ScCO_2$-DFA that interacts with vascular progenitor cells and examine their chemotactic properties. In addition, in this study, although vascular reflexes were observed in the $ScCO_2$-DFA after 90 days of XTP, the intensity of such reflexes was still far from that of the naïve vascular reflexes. Therefore, a combination of different strategies is required to bridge the gap between the biological vascular graft and the naïve vessel. Treatment strategies utilizing a stem cell chemoattractant, stem cell therapy after vascular implantation, and development of drug-coated vascular grafts are the different methods that can be used to bridge this gap.

CD34 is a protein expressed by hematopoietic stem cells and vascular progenitor cells,[36] and it does not appear on the surface of matured blood cells and vascular cells. The function of CD34 is complex and still not fully elucidated; Scientists now understand that the main function of CD34 is to participate in cell adhesion.[37] CD34-postive progenitor cells are collections of various cells, including EPCs and smooth muscle progenitor cells (SMPCs). EPCs have the functions of angiogenesis and repairing damaged vascular endothelium, while SMPCs are necessary members to maintain the vascular structure and tension. When damaged blood vessels need to be repaired or tissues need angiogenesis, EPCs and SMPCs should play their respective roles and differentiate in their appropriate locations. At this time, the CD34-postive progenitor cells in peripheral blood will be chemoattracted by many cytokines and proteins and homed to the target area through the adhesion function provided by CD34; The CD34-postive progenitor cells homing to the target tissue should be differentiated into endothelial cells and smooth muscle cells under suitable environments and surrounding conditions, and should complete different vascular functions.

Endothelial-to-mesenchymal transition (EndoMT) is the process of endothelial cells transdifferentiating to mesenchymal cells (including smooth muscle cells and fibroblasts);[38,39] This process is regulated by the transforming growth factor-β (TGF-β) signaling pathway and is closely related to tissue fibrosis.[39,40] Under normal conditions, bone marrow EPCs ($CD133^+CD34^+Flk1^+$) and circulating EPCs ($CD31^+$ $CD146^+vWF^+NOS^+$) have reendothelialization properties[41] that they are involved in the regular endothelial degeneration and regeneration processes of vessels. Since EPCs can adhere to the damaged endothelium and promote endothelial healing and repair,[42] they can maintain a balanced state of endothelial function.[43] Previous studies have also demonstrated that higher amounts of circulating EPCs can reduce the incidence of cardiovascular diseases and abnormal intimal hyperplasia after endothelium damage.[44] However, recent studies have found the opposite phenomenon that organ transplant recipients' EPCs are involved in the pathological process of allograft vasculopathy.[43,45,46] In the literature, the number of circulating EPCs in the patients with allograft vasculopathy was significantly higher than that in cases without allograft vasculopathy after transplantation.[47] The recipient's EPCs will adhere to the arterial vessel wall of the implanted organ and begin to proliferate, resulting in a sustained alloimmune response after transplantation.[45] In addition, EPCs accumulate uncontrollably and induce an immune response and subsequent proliferation of vascular smooth muscle cells, which in turn secrete large amounts of the extracellular matrix and lead to neointimal fibrosis.[43] Further studies have found that the cause of this phenomenon is the inappropriate environment caused by the immune inflammatory response, which in turn induces endoMT.[45,47] There is growing evidence that endoMT is closely related to atherosclerosis, pulmonary hypertension, vascular remodeling, vascular fibrosis, and heart valve diseases. This family of TGF-β-based proteins is considered to be the main regulator of endoMT, which contains four isoforms of TGF-β,[48,49] bone morphogenetic proteins (BMPs), and activins. TGF-β and BMP and activin receptor-like kinases (ALKs) form receptor complexes that regulate gene expression through phosphorylation of SMAD transcription factors.[50] The phosphorylated SMAD enters the nucleus and interacts with key transcription factors regulating endoMT (including SNAI1, SNAI2, ZEB1, ZEB2, KLF4, TCF3 and TWIST), ultimately leading to chromatin rearrangement and endoMT-related gene activation.[50] The molecular signaling system of endoMT also includes many factors that inhibit molecular signaling, such as BMP7[48] and SMAD7.[51] The TGF-β signaling pathway also interacts with many other signaling pathways, including mitogen-activated protein kinases, phosphoinositide 3-kinase pathways, microRNAs, and others. Therefore, in addition to the direct signaling induced by TGF-β, TGF-β also integrates other pathways and regulates the final changes of endoMT.[51]

Our LC-MS analysis results showed that the ScCO2-DFA retained a variety of proteins that could bind to CD34-postive progenitor cells, including lamin A/C, periostin, vimentin, desmin, biglycan, and integrin β. We also showed that the $ScCO_2$-DFA can attract more CD34-postive progenitor cells homing in immunofluorescent stained slides. The $ScCO_2$-DFA provided a better environment than the SDS-DFA and a lower level of inflammation/rejection to avoid the occurrence of EndoMT. We speculate that this is the reason why the smooth muscle cell layer in the $ScCO_2$-DFA can grow and differentiate well without excessive accumulation. Of course, an appropriate environment can also prompt the EPCs to secrete paracrine factors to inhibit inflammation and promote angiogenesis. Furthermore, less inflammation of the implant may indirectly induce less rejection and less inflammation in the spleen which we speculate. It is not yet known how the $ScCO_2$-DFA does not induce severe inflammatory reactions in the spleen

and how to provide a better environment for cell differentiation in the graft, so we need to perform more experiments to confirm it. In addition, the development of a graft that can effectively attract vascular progenitor cells, combined with stem cell-driven drugs, anti-inflammatory/anti-rejection drugs, and anti-EndoMT drugs is a possible direction for future treatment of vascular diseases.

5. Conclusion

$ScCO_2$ has been used to produce biological scaffolds in previous studies, and this is the first report on the use of $ScCO_2$ to produce vascular grafts, which have been used for XTP in a clinical setting. Our results showed that the $ScCO_2$-DFA induced low levels of inflammatory and immune-rejection responses, exhibited chemotaxis of vascular progenitor cells, and efficiently developed into a functional vasculature after XTP. Therefore, we believe that the use of $ScCO_2$ to fabricate decellularized biological vascular scaffolds can compensate for the limitations of current synthetic and biological vascular grafts.

Author contributions

S. Y. Sung, F. Y. Lin, C. C. Wu and Y. W. Lin conceived the project, designed and performed the experiments and analyzed the data. S. Periasamy, B. Nagarajan, and D. J. Hsieh contributed with regard to materials and consultation. S. Y. Sung, F. Y. Lin and Y. W. Lin contributed to the statistical analyses. S. Y. Sung and F. Y. Lin drafted the manuscript. C. Y. Lin and P. S. Hsua provided the consultation. Y. T. Tsai, C. S. Tsai and F. Y. Lin were the correspondents. All authors reviewed and approved the final version of the manuscript.

Conflicts of interest

There are no conflicts to declare.

Acknowledgements

We thank Shu-Wei Wu and Tze-Liang Yang for excellent technical assistance. This work was supported by National Science and Technology Council (MOST 110-2320-B-038-032-MY3), Tri-Service General Hospital (TSGH-D-109158, TSGH-C05-111039, TSGH-C05-111041) and Medical Affairs Bureau, Ministry of National Defense (MND-MAB-D-112175, D-MAB-C-11114-111051) in Taiwan.

References

1 N. Zea, G. Menard, L. Le, Q. Luo, H. A. Bazan, W. C. Sternberg 3rd and T. A. Smith, *Ann. Vasc. Surg.*, 2016, **30**, 28–33.
2 S. M. Gage and J. H. Lawson, *J. Vasc. Access*, 2017, **18**, 56–63.
3 E. Benrashid, C. C. McCoy, L. M. Youngwirth, J. Kim, R. J. Manson, J. C. Otto and J. H. Lawson, *Methods*, 2016, **99**, 13–19.
4 L. Gui, A. Muto, S. A. Chan, C. K. Breuer and L. E. Niklason, *Tissue Eng., Part A*, 2009, **15**, 2665–2676.
5 C. Quint, Y. Kondo, R. J. Manson, J. H. Lawson, A. Dardic and L. E. Niklason, *Proc. Natl. Acad. Sci. U. S. A.*, 2011, **108**, 9214–9219.
6 J. H. Lawson, M. H. Glickman, M. Ilzecki, T. Jakimowicz, A. Jaroszynski, E. K. Peden, A. J. Pilgrim, H. L. Prichard, M. Guziewicz, S. Przywara, J. Szmidt, J. Turek, W. Witkiewicz, N. Zapotoczny, T. Zubilewicz and L. E. Niklason, *Lancet*, 2016, **387**, 2026–2034.
7 H. Bai, A. Dardik and Y. Xing, *J. Surg. Res.*, 2019, **234**, 33–39.
8 H. Bai, Z. Wang, M. Li, P. Sun, W. Wang, W. Liu, S. Wei, Z. Wang, Y. Xing and A. Dardik, *Vascular*, 2020, **28**, 664–672.
9 S. Pashneh-Tala, S. MacNeil and F. Claeyssens, *Tissue Eng., Part B*, 2016, **22**, 68–100.
10 C. H. Lin, Y. C. Kao, Y. H. Lin, H. Ma and R. Y. Tsay, *Acta Biomater.*, 2016, **46**, 101–111.
11 P. M. Crapo, T. W. Gilbert and S. F. Badylak, *Biomaterials*, 2011, **32**, 3233–3243.
12 J. Negishi, S. Funamoto, T. Kimura, K. Nam, T. Higami and A. Kishida, *J. Tissue Eng. Regener. Med.*, 2015, **9**, E144–E151.
13 S. Funamoto, K. Nam, T. Kimura, A. Murakoshi, Y. Hashimoto, K. Niwaya, S. Kitamura, T. Fujisato and A. Kishida, *Biomaterials*, 2010, **31**, 3590–3595.
14 C. H. Lin, K. Hsia, H. Ma, H. Lee and J. H. Lu, *Int. J. Mol. Sci.*, 2018, **19**, 2101.
15 N. Das, M. J. Bratby, V. Shrivastava, A. J. Cornall, C. R. Darby, P. Boardman, S. Anthony and R. Uberoi, *Cardiovasc. Intervent. Radiol.*, 2011, **34**, 958–963.
16 S. Li and J. J. Henry, *Annu. Rev. Biomed. Eng.*, 2011, **13**, 451–475.
17 A. Gilpin and Y. Yang, *BioMed Res. Int.*, 2017, **2017**, 9831534.
18 S. Guler, B. Aslan, P. Hosseinian and H. M. Aydin, *Tissue Eng., Part C*, 2017, **23**, 540–547.
19 A. Gil-Ramirez, O. Rosmark, P. Spegel, K. Sward, G. Westergren-Thorsson, A. K. Larsson-Callerfelt and I. Rodriguez-Meizoso, *Sci. Rep.*, 2020, **10**, 4031.
20 C. E. Schmidt and J. M. Baier, *Biomaterials*, 2000, **21**, 2215–2231.
21 C. M. Liang, D. J. Hsieh, F. W. Tseng, P. Srinivasan, M. L. Yeh and M. C. Tai, *Cornea*, 2022, **41**, 328–338.
22 D. J. Hsieh and P. Srinivasan, *BioTechniques*, 2020, **69**, 220–225.
23 D. J. Hsieh, P. Srinivasan, K. C. Yen, Y. C. Yeh, Y. J. Chen, H. C. Wang and Y. W. Tarng, *BioTechniques*, 2021, **70**, 107–115.
24 L. Pu, J. Wu, X. Pan, Z. Hou, J. Zhang, W. Chen, Z. Na, M. Meng, H. Ni, L. Wang, Y. Li and L. Jiang, *J. Biomed. Mater. Res., Part B*, 2018, **106**, 619–631.

25 F. Y. Lin, C. M. Shih, C. Y. Huang, Y. T. Tsai, S. H. Loh, C. Y. Li, C. Y. Lin, Y. W. Lin and C. S. Tsai, *Cardiovasc. Drugs Ther.*, 2021, **35**, 1111–1127.
26 C. C. Shih, L. P. Hsu, M. H. Liao, S. S. Yang, S. T. Ho and C. C. Wu, *Eur. J. Pharmacol.*, 2017, **814**, 248–254.
27 S. O. Bello, E. W. Peng and P. K. Sarkar, *J. Cardiovasc. Med.*, 2011, **12**, 411–421.
28 P. Klinkert, P. N. Post, P. J. Breslau and J. H. van Bockel, *Eur. J. Vasc. Endovasc. Surg.*, 2004, **27**, 357–362.
29 F. D. Loop, *Ann. Thorac. Surg.*, 2005, **79**, S2221–S2227.
30 F. D. Loop, B. W. Lytle, D. M. Cosgrove, R. W. Stewart, M. Goormastic, G. W. Williams, L. A. Golding, C. C. Gill, P. C. Taylor, W. C. Sheldon, *et al.*, *N. Engl. J. Med.*, 1986, **314**, 1–6.
31 J. Lin, R. Guidoin, L. Wang, Z. Zhang, M. Nutley, R. Paynter, D. Wei, T. How, H. Crepeau, Y. Douville, G. Samis, G. Dionne and N. Gilbert, *J. Long-Term Eff. Med. Implants*, 2013, **23**, 67–86.
32 S. K. Gupta, N. C. Mishra and A. Dhasmana, *Methods Mol. Biol.*, 2018, **1577**, 1–10.
33 J. P. Zambon, A. Atala and J. J. Yoo, *Methods*, 2020, **171**, 3–10.
34 C. Philips, F. Campos, A. Roosens, M. D. C. Sanchez-Quevedo, H. Declercq and V. Carriel, *Ann. Biomed. Eng.*, 2018, **46**, 1921–1937.
35 U. Mendibil, R. Ruiz-Hernandez, S. Retegi-Carrion, N. Garcia-Urquia, B. Olalde-Graells and A. Abarrategi, *Int. J. Mol. Sci.*, 2020, **21**, 5447.
36 L. E. Sidney, M. J. Branch, S. E. Dunphy, H. S. Dua and A. Hopkinson, *Stem Cells*, 2014, **32**, 1380–1389.
37 B. Strilic, T. Kucera, J. Eglinger, M. R. Hughes, K. M. McNagny, S. Tsukita, E. Dejana, N. Ferrara and E. Lammert, *Dev. Cell*, 2009, **17**, 505–515.
38 L. A. Borthwick, S. M. Parker, K. A. Brougham, G. E. Johnson, M. R. Gorowiec, C. Ward, J. L. Lordan, P. A. Corris, J. A. Kirby and A. J. Fisher, *Thorax*, 2009, **64**, 770–777.
39 P. Y. Chen, L. Qin, C. Barnes, K. Charisse, T. Yi, X. Zhang, R. Ali, P. P. Medina, J. Yu, F. J. Slack, D. G. Anderson, V. Kotelianski, F. Wang, G. Tellides and M. Simons, *Cell Rep.*, 2012, **2**, 1684–1696.
40 S. Piera-Velazquez and S. A. Jimenez, *Fibrog. Tissue Repair*, 2012, **5**, S7.
41 J. L. Hillebrands, G. Onuta and J. Rozing, *Trends Cardiovasc. Med.*, 2005, **15**, 1–8.
42 D. A. D'Alessandro, J. Kajstura, T. Hosoda, A. Gatti, R. Bello, F. Mosna, S. Bardelli, H. Zheng, D. D'Amario, M. E. Padin-Iruegas, A. B. Carvalho, M. Rota, M. O. Zembala, D. Stern, O. Rimoldi, K. Urbanek, R. E. Michler, A. Leri and P. Anversa, *Circ. Res.*, 2009, **105**, 1128–1140.
43 J. L. Hillebrands, F. A. Klatter and J. Rozing, *Arterioscler., Thromb., Vasc. Biol.*, 2003, **23**, 380–387.
44 J. M. Hill, G. Zalos, J. P. Halcox, W. H. Schenke, M. A. Waclawiw, A. A. Quyyumi and T. Finkel, *N. Engl. J. Med.*, 2003, **348**, 593–600.
45 C. J. Sathya, R. Sheshgiri, J. Prodger, L. Tumiati, D. Delgado, H. J. Ross and V. Rao, *Transplant Int.*, 2010, **23**, 641–648.
46 M. J. Weiss, J. C. Madsen, B. R. Rosengard and J. S. Allan, *Front. Biosci.*, 2008, **13**, 2980–2988.
47 D. Simper, S. Wang, A. Deb, D. Holmes, C. McGregor, R. Frantz, S. S. Kushwaha and N. M. Caplice, *Circulation*, 2003, **108**, 143–149.
48 E. M. Zeisberg, O. Tarnavski, M. Zeisberg, A. L. Dorfman, J. R. McMullen, E. Gustafsson, A. Chandraker, X. Yuan, W. T. Pu, A. B. Roberts, E. G. Neilson, M. H. Sayegh, S. Izumo and R. Kalluri, *Nat. Med.*, 2007, **13**, 952–961.
49 S. M. Evrard, L. Lecce, K. C. Michelis, A. Nomura-Kitabayashi, G. Pandey, K. R. Purushothaman, V. d'Escamard, J. R. Li, L. Hadri, K. Fujitani, P. R. Moreno, L. Benard, P. Rimmele, A. Cohain, B. Mecham, G. J. Randolph, E. G. Nabel, R. Hajjar, V. Fuster, M. Boehm and J. C. Kovacic, *Nat. Commun.*, 2016, **7**, 11853.
50 R. Derynck and Y. E. Zhang, *Nature*, 2003, **425**, 577–584.
51 J. Xiong, H. Kawagishi, Y. Yan, J. Liu, Q. S. Wells, L. R. Edmunds, M. M. Fergusson, Z. X. Yu, I. I. Rovira, E. L. Brittain, M. J. Wolfgang, M. J. Jurczak, J. P. Fessel and T. Finkel, *Mol. Cell*, 2018, **69**, 689–698.